Original Article

Determining the invasiveness of pure ground-glass nodules using dual-energy spectral computed tomography

Ye Yu[1#], Jie-Jun Cheng[1#], Jian-Ying Li[2], Ying Zhang[1], Liao-Yi Lin[1], Feng Zhang[1], Jian-Rong Xu[1], Xiao-Jing Zhao[3], Hua-Wei Wu[1]

[1]Department of Radiology, Renji Hospital, School of Medicine, Shanghai Jiaotong University, Shanghai 200000, China; [2]CTRC, General Electric Company Healthcare China, Shanghai 200000, China; [3]Department of Thoracic Surgery, Renji Hospital, School of Medicine, Shanghai Jiaotong University, Shanghai 200000, China

Contributions: (I) Conception and design: Y Yu, JJ Cheng, HW Wu; (II) Administrative support: JR Xu, HW Wu; (III) Provision of study materials or patients: XJ Zhao; (IV) Collection and assembly of data: Y Yu, JJ Cheng, Y Zhang, LY Lin; (V) Data analysis and interpretation: Y Yu, JJ Cheng, JY Li; (VI) Manuscript writing: All authors; (VII) Final approval of manuscript: All authors.

[#]These authors contributed equally to this work.

Correspondence to: Xiao-Jing Zhao. Department of Thoracic Surgery, Renji Hospital, School of Medicine, Shanghai Jiaotong University, Shanghai 200000, China. Email: drzhaoxiaojing@aliyun.com; Hua-Wei Wu. Department of Radiology, Renji Hospital, School of Medicine, Shanghai Jiaotong University, Shanghai 200000, China. Email: huaweiwu26@163.com.

Background: The present work aimed to investigate the clinical application of using quantitative parameters generated in the unenhanced phase (UP) and venous phase (VP) in dual-energy spectral CT for differentiating the invasiveness of pure ground-glass nodule (pGGN).

Methods: Sixty-two patients with 66 pGGNs who underwent preoperative dual-energy spectral CT in UP and VP were evaluated retrospectively. Nodules were divided into three groups based on pathology: adenocarcinoma in situ (AIS, n=19), minimally invasive adenocarcinoma (MIA, n=22) (both in the preinvasive lesion group) and invasive adenocarcinoma (IA, n=25). The iodine concentration (IC) and water content (WC) in nodules were measured in material decomposition images. The nodule CT numbers and slopes(k) were measured on monochromatic images. All measurements, including the maximum diameter of nodules were statistically compared between the AIS-MIA group and IA group.

Results: There were significant differences of WC in VP between AIS-MIA group and IA group ($P<0.05$). The CT attenuation values of the 40–140 keV monochromatic images in UP and VP were significantly higher for the invasive nodules. Logistic regression analysis showed that the maximum nodule diameter [odd ratio (OR) =1.21, 95% CI: 1.050–1.400, $P<0.01$] and CT number in 130 keV images in venous phase (OR =1.03, 95% CI: 1.014–1.047, $P<0.001$) independently predicted histological invasiveness.

Conclusions: The quantitative parameters in dual-energy spectral CT in the unenhanced phase and venous phase provide useful information in differentiating preinvasive lesion group from IA group of pGGN, especially the maximum nodule diameter and CT number in the 130 keV images in the venous phase.

Keywords: Dual-energy; ground-glass nodule (GGN); invasiveness; lung adenocarcinoma; spectral CT

Submitted Oct 09, 2019. Accepted for publication Mar 13, 2020.

doi: 10.21037/tlcr.2020.03.33

View this article at: http://dx.doi.org/10.21037/tlcr.2020.03.33

Introduction

With the application of high-resolution computed tomography (CT), more and more ground-glass opacity nodules are being detected. Ground-glass nodule (GGN) on CT is defined as hazy increased density of the lungs, but with presentation of bronchial and vascular margins (1). GGN is classified into pure ground-glass nodule (pGGN), which has no solid components, and part-solid nodules (PSNs), with solid components (2). In some articles, the ratio of solid components is studied, and the more the solid components are included, the more malignancy it may be (3,4).

Though many diseases either benign or malignancy can manifest as GGN, it is reported that lung adenocarcinoma often appears as localized GGNs on CT, and lung adenocarcinoma is becoming the main pathology type of lung cancer. According to the classification on lung adenocarcinoma proposed in 2011 (5) and adopted by WHO in 2015 (6), adenocarcinoma is classified into atypical adenomatous hyperplasia (AAH), adenocarcinoma *in situ* (AIS), minimally invasive adenocarcinoma (MIA) and invasive adenocarcinoma (IA). On one hand, the AIS and MIA had similar prognoses, with 100% disease-specific survival (5). While for IA, the 5-year overall survival is about 49–84% (7). On the other hand, even though the resection for the entire group of lymph node or lobectomy is still the standard surgical treatment of IA, patients with AIS or MIA can accept wedge or segment resection to maintain lung function and reduce incidence and mortality. For pGGN, approximately 30–40% of all resected pGGNs were IAs in some studies (8-10). Therefore, it is important to be able to differentiate the invasiveness of pGGNs.

In recent years the dual-energy spectral CT, which extends the capabilities of conventional CT, has emerged as a promising non-invasive imaging method in clinical work. It provides material decomposition images and virtual monochromatic images for quantification, the parameters including iodine concentration (IC) and water content (WC) from material decomposition images, CT attenuation value (CT number) measurements from the 101 sets of virtual monochromatic images (40–140 keV photon energy) (11). Many researchers have already investigated the value of GGN morphology (12-16) and several quantitative CT features for predicting the invasiveness of lung pure ground-glass nodules on conventional CT (17). In addition, researchers have already used quantitative CT parameters (i.e. volume doubling time and mass doubling time) for predicting the behavior of persistent GGNs and the controversial role of doubling time (DT) in predicting the invasiveness of adenocarcinomas presenting as GGNs (18-20). However, there are few research about using dual-energy spectral CT to analyze GGN, especially about pGGN. So, the purpose of our study was to investigate the clinical application of using the quantitative parameters generated in the unenhanced phase and venous phase in dual-energy spectral CT for differentiating the invasiveness of pure ground-glass nodules (pGGNs).

Methods

Subjects

We retrospectively analyzed 62 patients with 66 pure ground-glass nodules (58 patients with single lesion, 4 patients with 2 lesions) who underwent both the unenhanced and the contrast-enhanced dual-energy spectral CT from April 2016 to May 2019 in our hospital (*Figure 1* shows the flowchart of study population). These patients were identified by pathology as having pGGN. Of the 62 patients, 43 were females and 19 were males, with age ranging from 29 to 75 years and mean age of 55.4 years. The inclusion criteria were: (I) nodules were pathologically confirmed and without solid components; (II) nodules with diameters of 3 cm or less in their largest dimension (lesion size was measured on thin-section images).

CT examination

The unenhanced and contrast-enhanced dual-energy spectral CT scans of the lungs were performed on a 64-slice CT scanner (Discovery CT750HD, GE Healthcare, Waukesha USA) using the following scan protocol: (I) spectral imaging mode with single-source, fast tube voltage switching between 80 and 140 kVp on adjacent views; (II) 0.6 seconds tube rotation time; (III) 275 mA tube current; (IV) 1.375:1 helical pitch; (V) 500 mm scan field of view; (VI) 1.25 mm slice thickness and image interval. For the contrast-enhanced CT scan, all patients were injected with non-ionic iodinated contrast material with 370 mg/mL concentration (Iopamidol, Shanghai Bracco Sine Pharmaceutical, Shanghai, China) at a dose of 1.35 mL/kg body weight and a contrast injection rate of 3.0 mL/s by using a power injector (OptiVantage, Tyco Healthcare, Cincinnati). The venous phase (VP) scan started at 65 seconds after the beginning of contrast injection.

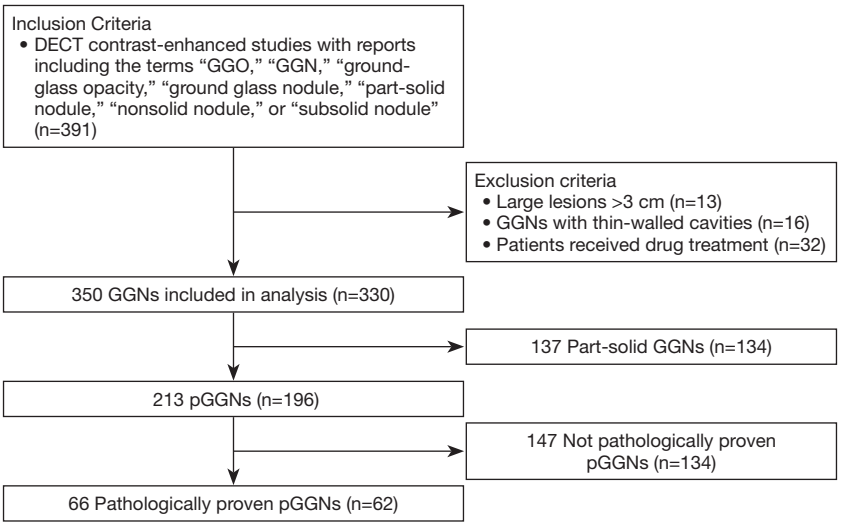

Figure 1 Flowchart shows study population. Numbers in parentheses are number of patients. DECT, dual-energy CT; GGO, ground-glass opacity; GGN, ground glass nodule; pGGN, pure ground-glass nodule.

Imaging analysis

Two types of images were reconstructed from the single dual-energy spectral CT scan: iodine and water-based material decomposition images and 101 sets of virtual monochromatic images with photon energies from 40–140 keV at 1 keV interval. These images were transferred to an advanced workstation (ADW4.6; GE Healthcare) with Gemstone Spectral Imaging (GSI) Viewer software (GE Healthcare) for analysis.

Two radiologists unaware of patients' information and pathologic results interpreted the images and measured the quantitative parameters on the monochromatic and material decomposition images in the unenhanced phase and venous phase on ADW4.6 independent of each other. The principles for the measurement of pGGN were as following: (I) Selecting three slices containing pGGN; (II) selecting a region-of-interest (ROI) covering more than 70% of the lesion area in the maximum section for the lesion and avoid major vessels and bubbles. The size, shape, and position of the ROIs in different image types and phases were kept consistent using the copy and paste function as far as possible. Measurements were performed three times in the three consecutive axial sections to obtain average values for the individual reviewer. And finally, the average values for the two reviewers were calculated and used for analysis and comparison among different lesion types. The measurements included the CT attenuation values (CT numbers) of pGGN using the 40–140 keV virtual monochromatic images and their iodine concentration (IC) and water content (WC) from the iodine-based and water-based material decomposition images, respectively in both the unenhanced and venous phases. To minimize the influence of the individual circulation status and scanning times, the IC values of lesions were normalized to that of the aorta in the same section to calculate the normalized iodine concentration (NIC): NIC = IClesion/ICaorta. The slope(k) of the CT number as function of photon energy curve was calculated using the 101 sets of monochromatic images: slope(k) = |CT number (40 keV) – CT number (100 keV)|/60.

Statistical analysis

All data were analyzed using a commercial statistical software package (version 22.0, SPSS IBM; MedCalc, version 12.0, MedCalc Software, Mariakerke, Belgium; GraphPad Prism version 6, GraphPad Software, La Jolla, California, USA), A P value of <0.05 was considered statistically significant.

In all, the maximum diameter of nodules, IC, NIC, the slope(k), WC and CT numbers of monochromatic images at 40–140 keV in two phases were obtained. The results were expressed as mean ± standard deviation. In addition, because AIS and MIA had similar prognoses, these two subtypes of pGGNs were combined into AIS-MIA group and compared with IA group. Normality of variance was assessed by the one-sample Kolmogorov-Smirnov (K-S) test. For normally

Table 1 Clinical characteristics of patients

Characteristics	Data
Patients total number	62
Gender, n (%)	
Male	19 (30.6)
Female	43 (69.4)
Smoking, n (%)	
Smoker	4 (6.5)
No smoker	58 (93.5)
Age (year)	55.4±11.6
GGN total number	66
GGN location, n (%)	
RUL	26 (39.4)
RML	2 (3.0)
RLL	10 (15.2)
LUL	18 (27.2)
LLL	10 (15.2)
Histological types, n (%)	
AIS	19 (28.8)
MIA	22 (33.3)
IA	25 (37.9)

GGN, ground-glass nodule; RUL, right upper lobe; RML, right middle lobe; RLL, right lower lobe; LUL, left upper lobe; LLL, left lower lobe; AIS, adenocarcinoma in situ; MIA, minimally invasive adenocarcinoma; IA, invasive adenocarcinoma.

distributed continuous variables, independent-samples t-test was used. Non-normally distributed continuous variables were analyzed by the non-parametric K-S test. The significant factors in the univariate analysis were identified as candidate covariates in a logistic regression model with forward stepwise selection, and odds ratios (ORs) were calculated. Furthermore, receiver operating characteristic (ROC) analysis was performed to evaluate the performance of spectral CT parameters in differentiating the AIS-MIA group from IA group.

Results

Patients

Sixty-two patients underwent dual-energy spectral CT examination were included in the study. There were 66 pGGNs (58 patients with single lesion, 4 patients with 2 lesions) identified by pathology after CT examination. Among the 66 pGGNs, 19 were AIS, 22 were MIA and 25 were IA. The clinical characteristics of the 62 patients are summarized in *Table 1*.

Inter-observer agreement

Interobserver agreement for measurements is shown in *Table 2*.

Relationships between pathology and Dual-energy spectral CT findings

The CT numbers at 40–140 keV in both phases had statistically significant difference between preinvasive lesion group and IA group (*Tables 3*,*4*).

The comparison of the material density measurements of pGGNs with different invasiveness is shown in *Table 5* and *Figure 2*. There were significant differences in the water content in venous phase, and the maximum diameter of pGGNs between preinvasive lesion group and IA group. However, there was no difference in both the iodine concentration and normalized iodine concentration between them. For multivariate analysis, we used the parameters that were statistically significant in the univariate analysis. The results revealed that the maximum nodule diameter (odd ratio OR =1.21, 95% CI: 1.050–1.400, P<0.01) and the CT number in the 130keV images in venous phase (OR =1.03, 95% CI: 1.014–1.047, P<0.001) were independent predictors for the IA group. The area under the curve (AUC), sensitivity and specificity of the predictive model were 0.901, 84.00%, 82.93%, and showing higher AUC value than the maximum nodule diameter (AUC=0.786), or the CT number of the 130 keV images in venous phase (AUC=0.860) alone (*Table 6* and *Figure 3*). The two clinical cases are shown in *Figures 4* and *5*.

Discussion

The quantitative enhancement degree of lesion in conventional CT can reflect the blood supply and distribution in the intravascular and extracellular spaces and assess the benign or malignancy of lesions (21,22). With the development of technology, dual-energy spectral CT provides not only material concentrations using material decomposition images to better reflect the contrast-enhancement information, but also CT attenuation values

Table 2 Inter-observer agreement of variates

Variates	ICCs
Monochromatic CT number in unenhanced phase	
40 keV	0.8674
50 keV	0.9053
60 keV	0.9248
70 keV	0.9258
80 keV	0.9248
90 keV	0.9250
100 keV	0.9240
110 keV	0.9218
120 keV	0.9215
130 keV	0.9209
140 keV	0.9202
Monochromatic CT number in venous phase	
40 keV	0.8431
50 keV	0.9005
60 keV	0.9320
70 keV	0.9411
80 keV	0.9334
90 keV	0.9390
100 keV	0.9325
110 keV	0.9274
120 keV	0.9377
130 keV	0.9367
140 keV	0.9359
IC in venous phase	0.7191
WC in venous phase	0.8476
Slope(k) in venous phase	0.7863
Slope(k) in unenhanced phase	0.7731
NIC in venous phase	0.8072
Maximum nodule diameter	0.9320

ICC, intraclass correlation coefficient; CT, computed tomography; IC, iodine concentration; WC, water content; slope(k), slope of spectral curve; NIC, normalized iodine concentration.

from a set of virtual monochromatic images to be less influenced by beam hardening effects as in the conventional CT. The material decomposition images can be used to estimate quantitatively the water and iodine content (23) in lesions. In addition, monochromatic image sets provide information about the attenuation changes of different materials as a function of X-ray photon energy. However, a few researchers have analyzed the GGN using dual-energy spectral CT. Son *et al.* (24) found that combining texture analyze with dual-energy spectral CT, the iodine-enhanced imaging metrics versus virtual non-contrast (VNC) imaging metrics have added value in distinguishing IA from AIS or MIA. But it was difficult and tedious in clinical application. Recently, Liu *et al.* (25) confirmed that tumorous GGN has blood supply. But they didn't analyze the invasiveness of GGNs. Other researchers (26) studied the CT attenuation of pGGN in a series of enhanced monochromatic energies and found that monochromatic CT number of higher energy (especially 140 keV) would be better for diagnosing IA than lower energies. Whereas they only analyzed the delayed phase images. Yang *et al.* (27) proposed modified NIC to differentiating IAs from preinvasive lesions using a dual-source, dual-energy approach, and the study design was rather complicated. Unlike those previous studies, we further performed quantitative analysis of iodine concentration, normalized iodine concentration, water content and monochromatic CT numbers in both the unenhanced phase and venous phase using a single-source dual-energy approach. Similar to the previous studies (28), we found that the most common sub-types of pGGN in our study were AIS and MIA.

Histologically, GGN is the partial filling of the terminal air spaces, interstitial thickening by fluid, cells, fibrosis and increased capillary blood volume, or a combination of these factors (29,30). Interestingly, we found that IC and NIC in the venous phase had no significance in indicting the degrees of invasion. The iodine concentration is often used to reflect the blood flow in contrast-enhanced CT scans, since iodine is the most commonly used contrast agent (31). The no difference finding in IC may indicate that the blood supply to pGGN of different types was not high enough or different enough to be differentiated.

On the other hand, the intrinsic structures or densities of pGGNs with different invasiveness may be different. In our study, we used the iodine-water base material pairs to represent the attenuation of nodules in the enhancement phase. The combination of these two materials reflected the detected density. Since iodine better represents the contrast medium that is in the nodule, the water content reflects the physical density of the GGN (32). Similarly to the previous study (25), we found that the water content in

Table 3 CT values (HU) of pGGN with different invasiveness at 40-140 keV in unenhanced phase (UP)

Photon energy	Preinvasive lesion group (n=41)		IA group (n=25)	P value
	AIS (n=19)	MIA (n=22)		
40 keV	−568.8±35.4	−565.5±59.8	−510.9±71.7	0.001
50 keV*	−614.3±30.4	−600.8±55.8	−544.6±68.3	0.005
60 keV*	−650.5±35.7	−628.7±53.9	−571.6±66.0	0.001
70 keV*	−666.2±36.4	−641.1±53.9	−582.9±65.9	<0.001
80 keV*	−670.2±36.1	−644.5±54.2	−586.1±66.2	<0.001
90 keV*	−676.4±36.5	−649.3±54.2	−591.8±65.6	<0.001
100 keV	−681.4±36.9	−653.2±54.3	−595.6±65.5	<0.001
110 keV	−684.7±37.8	−656.0±54.3	−598.3±65.4	<0.001
120 keV	−687.4±37.4	−658.0±54.5	−600.2±65.4	<0.001
130 keV	−689.3±37.6	−659.5±54.5	−601.0±65.3	<0.001
140 keV	−690.8±37.6	−660.6±54.6	−602.8±65.3	<0.001

*, non-parametric two-sample K-S test for non-normally distributed continuous data; pGGN, pure ground-glass nodule; AIS, adenocarcinoma in situ; MIA, minimally invasive adenocarcinoma; IA, invasive adenocarcinoma.

Table 4 CT value of every group at 40-140 kev in venous phase

Photon energy	Preinvasive lesion group (n=41)		IA group (n=25)	P value
	AIS (n=19)	MIA (n=22)		
40 keV*	−520.3±35.6	−491.2±67.9	−417.4±89.9	<0.001
50 keV*	−580.9±33.7	−549.4±62.4	−476.9±78.8	<0.001
60 keV	−626.2±34.7	−591.8 ±59.3	−519.5±71.6	<0.001
70 keV	−648. 9±35.5	−613.9±57.9	−541.2±69.0	<0.001
80 keV	−657.5±35.3	−623.8±57.7	−551.0±68.2	<0.001
90 keV	−665.8±35.5	−630.5±58.0	−560.3±66.6	<0.001
100 keV	−672.5±35.9	−637.5±57.3	−567.5±65.5	<0.001
110 keV	−677.4±36.2	−641.3±56.8	−571.4±65.3	<0.001
120 keV	−680.8±36.4	−645.4±57.1	−575.1±65.0	<0.001
130 keV	−683.3±36.6	−647.9±57.0	−577.6±64.7	<0.001
140 keV	−685.4±36.7	−649.7±56.9	−579.6±64.5	<0.001

*, non-parametric two-sample K-S test for non-normally distributed continuous data; CT, computed tomography; adenocarcinoma in situ; MIA, minimally invasive adenocarcinoma; IA, invasive adenocarcinoma.

both the unenhanced and contrast-enhanced venous phases had significantly differences between the preinvasive lesion group and IA group, and the IA group had the highest water content. Travis *et al.* (5) pointed out that tumor cells in pGGNs are usually distributed along pre-existing lung alveolar structures in a lepidic growth pattern, which present looseness. With the invasion of stroma, stromal proliferation, or framework collapse, the lesions become more compact. Since IA has more tumor cells proliferation and invasion, it is thus reasonable that IA is more compact and has higher density, thus higher water content in IA than in the pre-invasion nodules.

Table 5 Comparison of material density measurements of pGGNs with different invasiveness

Parameters	Preinvasive lesion group (n=41)		IA group (n=25)	P value
	AIS (n=19)	MIA (n=22)		
IC in VP (100 μg/mL)	21.7±3.9	21.1±4.1	21.1±5.0	0.820
NIC in VP	0.5±0.1	0. 5±0.1	0.4 ±0.1	0.113
WC in VP (mg/mL)	308.2±43.8	337.4 ±55. 5	409.2 ±63.1	<0.001
maximum nodule diameter (mm)*	7.2±1.8	11. 8±5.3	14.0±4.1	<0.001
Slope(k) in UP	1.9±0.4	1.5±0.5	1.4±0.4	0.042
Slope(k) in VP	2.5±0.4	2.4±0.5	2.5±0.7	0.900

*, non-parametric two-sample K-S test for non-normally distributed continuous data. pGGNs, pure ground-glass nodules; AIS, adenocarcinoma in situ; MIA, minimally invasive adenocarcinoma; IA, invasive adenocarcinoma; IC, iodine concentration; VP, venous phase; NIC, normalized iodine concentration; WC, water content; slope(k), slope of spectral curve; UP, unenhanced phase.

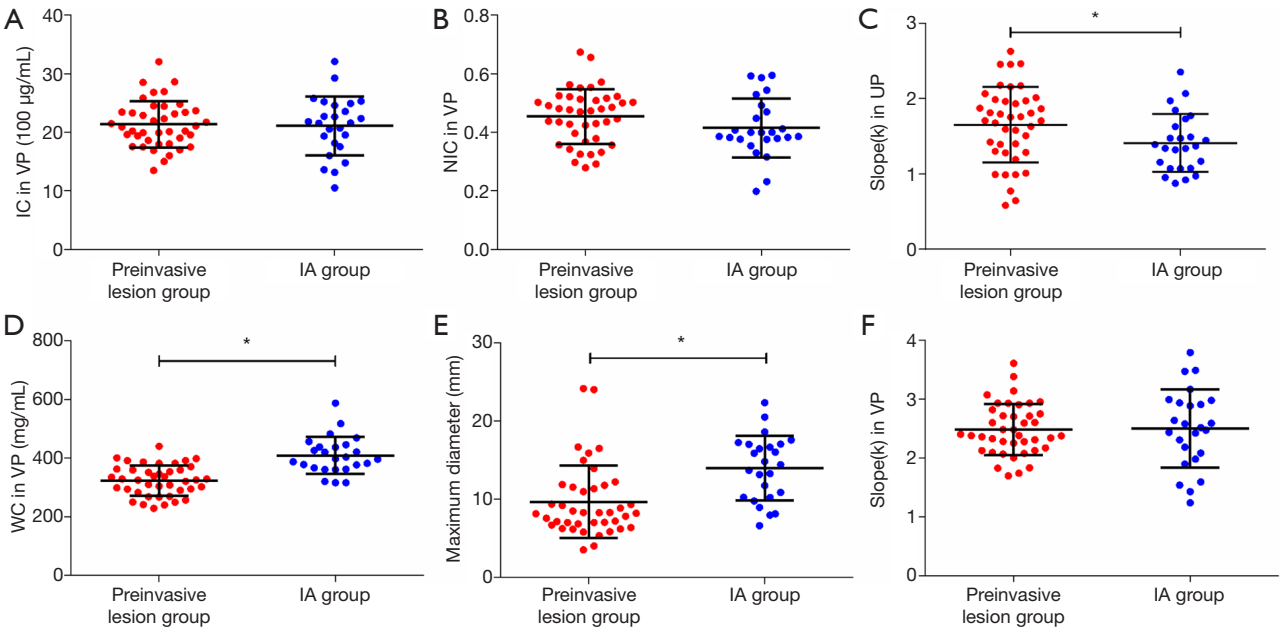

Figure 2 Comparison of Preinvasive lesion group and IA group. The asterisks represent the P values: *, P<0.05. (A) Comparison of IC in VP. (B) Comparison of NIC in VP. (C) Comparison of slope(k) in UP. (D) Comparison of WC in VP. (E) Comparison of the maximum nodule diameter. (F) Comparison of slope(k) in VP. IA, invasive adenocarcinoma; IC, iodine concentration; VP, venous phase; NIC, normalized iodine concentration; WC, water content; UP, unenhanced phase.

In our study, the maximum nodule diameter was shown to be an independent factor in discriminating IA with the cut-off value of 9.36 mm. In general, our findings are similar to the results of Lee *et al.* (28) and Jin *et al.* (9) that pGGNs with diameters of 10 or 10.5 mm are more likely to be IA, but a size measurement alone may not be reliable enough to indicate histopathologic subtypes.

One of the advantages of dual-energy spectral CT is that it produces a set of virtual monochromatic images from 40 to 140 keV photon energies and allows image interpretation at various energy levels from a single CT examination. Our results indicated that there were statistically significant differences in the CT number in the entire energy spectrum between the preinvasive lesion group and IA

Table 6 Diagnostic efficiencies of WC (in mg/mL) in the venous phase and CT number (in HU) at different energies in both the UP and VP in differentiating AIS and MIA from IA

Parameters	AUC	Sensitivity (%)	Specificity (%)	Threshold
WC in VP	0.856	88.0	75.6	360.0
maximum diameter	0.786	84.0	68.3	9.4
CT number at 40 keV in UP	0.719	52.0	92.7	–506.0
CT number at 40 keV in VP	0.794	64.0	87.8	–449.2
CT number at 50 keV in UP	0.763	68.0	75.6	–584.0
CT number at 50 keV in VP	0.829	84.0	75.6	–537.0
CT number at 60 keV in UP	0.798	76.0	75.6	–626.4
CT number at 60 keV in VP	0.853	84.0	78.1	–575.8
CT number at 70 keV in UP	0.813	84.0	73.1	–640.9
CT number at 70 keV in VP	0.859	84.0	75.6	–599.3
CT number at 80 keV in UP	0.817	84.0	73.1	–645.3
CT number at 80 keV in VP	0.858	84.0	75.6	–606.0
CT number at 90 keV in UP	0.816	72.0	82.9	–624.5
CT number at 90 keV in VP	0.857	84.0	78.1	–611.2
CT number at 100 keV in UP	0.820	72.0	82.9	–630.0
CT number at 100 keV in VP	0.859	88.0	73.2	–620.1
CT number at 110 keV in UP	0.822	72.0	82.9	–633.9
CT number at 110 keV in VP	0.858	88.0	75.6	–625.4
CT number at 120 keV in UP	0.824	72.0	82.9	–636.6
CT number at 120 keV in VP	0.861	88.0	75.6	–628.9
CT number at 130 keV in UP	0.825	76.0	80.5	–640.7
CT number at 130 keV in VP	0.860	88.0	75.6	–631.4
CT number at 140 keV in UP	0.827	76.0	82.9	–640.4
CT number at 140 keV in VP	0.861	88.0	75.6	–633.6
Independent predictors	0.901	84.0	82.9	–

WC, water content; CT, computed tomography; UP, unenhanced phase; VP, venous phase; AUC, area under curve.

group. We also found that the CT numbers of the higher energy monochromatic images had high diagnostic power in indicating IA. This finding is similar to that of Zhang *et al.* (26), whose study showed that the CT numbers of the 120–140 keV monochromatic images in the contrast-enhanced delay phase performed better than the CT numbers of the conventional nonenhanced polychromatic images to indicate IA. In dual-energy spectral CT, organs or lesions containing iodine appear denser in the low-keV images, but the image noise can also be much higher despite contrasting with the surrounding tissue is evident (33). On the other hand, the monochromatic images with high energy have better noise performance (34,35), and it is thus advantageous to be able to fully utilize high energy monochromatic images. We found that slope(k) in the unenhanced phase had significant difference in distinguishing IA group from preinvasive lesion group. In addition, we also showed that the monochromatic CT number had significant difference in distinguishing IA group from preinvasive lesion group in both the unenhanced phase and venous phase with dual energy CT, in the multivariate analysis, we found only CT numbers in the 130 keV images in venous phase was the predicting factor for IA.

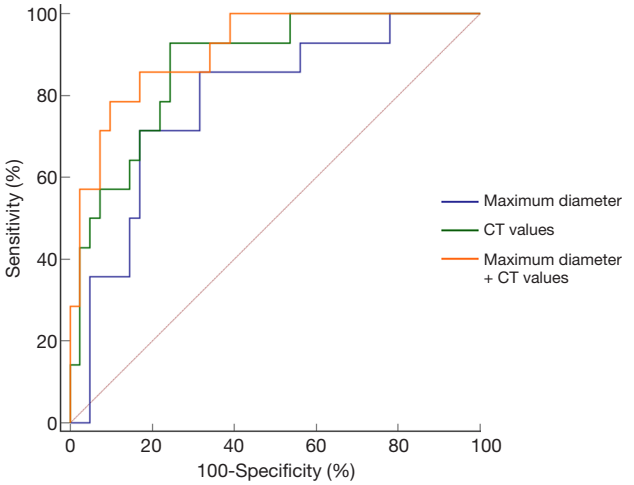

Figure 3 ROC curves for indicating invasive adenocarcinoma. ROC, receiver operating curve; CT, computed tomography.

There are some limitations in our study. Firstly, our results were limited by the relatively small sample size. More patients, especially patients with IA are needed in

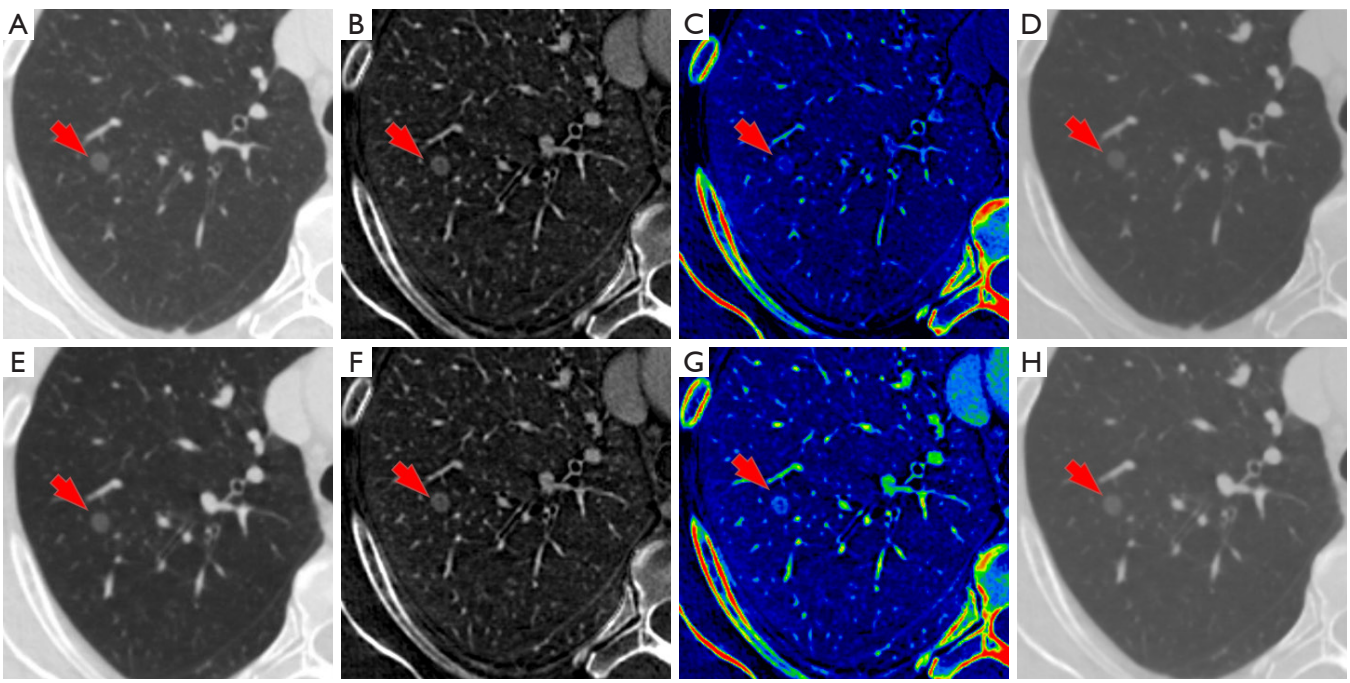

Figure 4 A 53-year-old woman with adenocarcinoma in situ, with maximum diameter of 7.6 mm. (A) Unenhanced image; (B,C) iodine image in unenhanced phase; (D) water image in unenhanced phase; (E) 130-keV monochromatic image in venous phase. The average CT attenuation value was –683.0 HU; (F,G) iodine image in venous phase, iodine concentration of lesion in venous phase was 24.62 (100 μg/mL); (H) water image in venous phase, water content of lesion in venous phase was 324.73 mg/mL. CT, computed tomography; HU, Hounsfield unit. Red arrows point out the lesions.

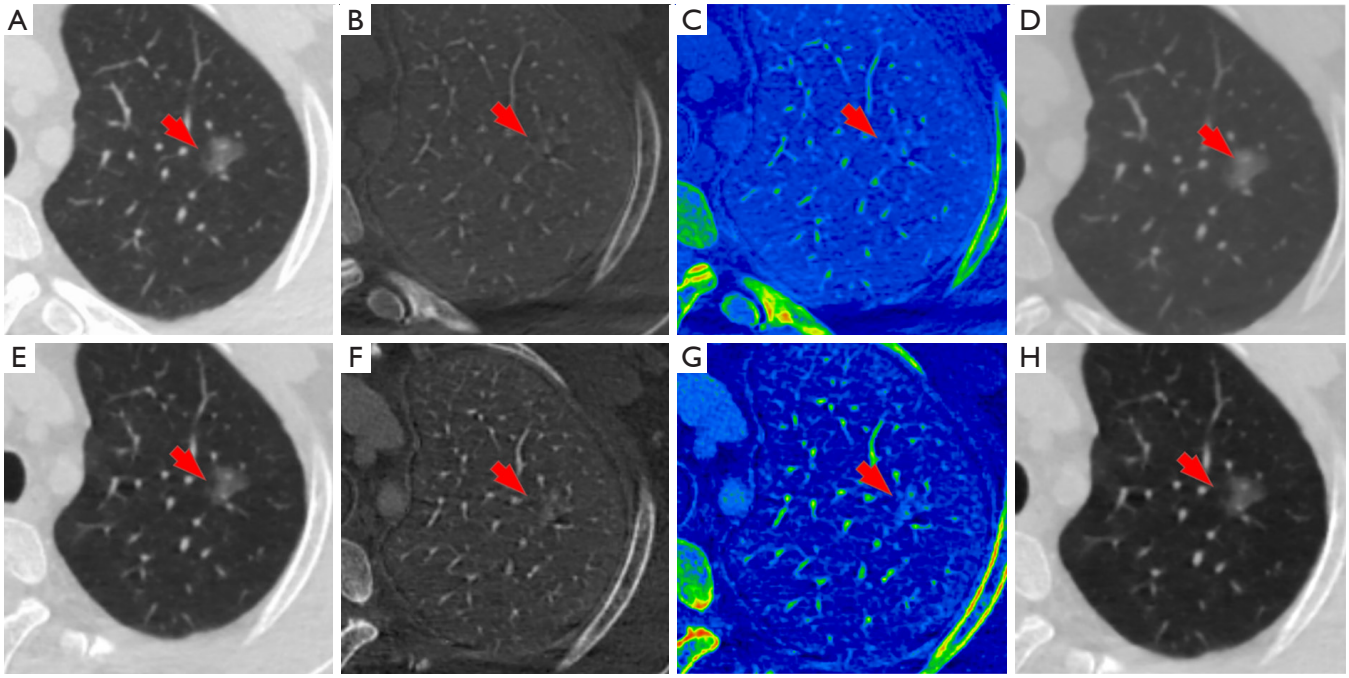

Figure 5 A 52-year-old man with invasive adenocarcinoma, with maximum diameter of 15.3 mm. (A) Unenhanced image; (B,C) iodine image in unenhanced phase; (D) water image in unenhanced phase; (E) 130-keV monochromatic image in venous phase. The average CT attenuation value was −565.6 HU; (F,G) iodine image in venous phase, iodine concentration of lesion in venous phase was 18.61 (100 μg/mL); (H) water image in venous phase, water content of lesion in venous phase was 463.72 mg/mL. CT, computed tomography; HU, Hounsfield unit. Red arrows point out the lesions.

future studies to improve the accuracy. Secondly, we only analyzed the maximum nodule diameter, CT number and material density parameters of pGGN, more morphology information will need to be added in the future. Thirdly, this was a retrospective and single institution study, and there existed patient selection bias.

Conclusions

Overall, the quantitative parameters in dual-energy spectral CT in the unenhanced phase and venous phase, together with the maximum diameter of lesions provide useful information in predicting IA, which manifested as pure ground-glass nodules.

Acknowledgments

Funding: This research was supported by the National Natural Science Foundation of China (Grant No.81571670).

Footnote

Conflicts of Interest: All authors have completed the ICMJE uniform disclosure form (available at http://dx.doi.org/10.21037/tlcr.2020.03.33). The authors have no conflicts of interest to declare.

Ethical Statement: The authors are accountable for all aspects of the work in ensuring that questions related to the accuracy or integrity of any part of the work are appropriately investigated and resolved. This research was conducted in accordance with the Declaration of Helsinki (as revised in 2013). This research was approved by the Institutional Ethics Board of Renji Hospital, School of Medicine, Shanghai Jiaotong University (No. 2017-082) and individual consent for this retrospective analysis was waived.

Open Access Statement: This is an Open Access article distributed in accordance with the Creative Commons

References

1. Henschke CI, Yankelevitz DF, Mirtcheva R, et al. CT screening for lung cancer: frequency and significance of part-solid and nonsolid nodules. AJR Am J Roentgenol 2002;178:1053-7.
2. Hansell DM, Bankier AA, MacMahon H, et al. Fleischner Society: glossary of terms for thoracic imaging. Radiology 2008;246:697-722.
3. Moon Y, Lee K, Park J. The prognosis of invasive adenocarcinoma presenting as ground-glass opacity on chest computed tomography after sublobar resection. J Thorac Dis 2017;9:3782-92.
4. Wu H, Liu C, Xu M, et al. A Retrospective Study of Mean Computed Tomography Value to Predict the Tumor Invasiveness in AAH and Clinical Stage Ia Lung Cancer. Zhongguo Fei Ai Za Zhi 2018;21:190-6.
5. Travis WD, Brambilla E, Noguchi M, et al. International association for the study of lung cancer/american thoracic society/european respiratory society international multidisciplinary classification of lung adenocarcinoma. J Thorac Oncol 2011;6:244-85.
6. Travis WD, Brambilla E, Nicholson AG, et al. The 2015 World Health Organization Classification of Lung Tumors: Impact of Genetic, Clinical and Radiologic Advances Since the 2004 Classification. J Thorac Oncol 2015;10:1243-60.
7. Van Schil PE, Asamura H, Rusch VW, et al. Surgical implications of the new IASLC/ATS/ERS adenocarcinoma classification. Eur Respir J 2012;39:478-86.
8. Lim HJ, Ahn S, Lee KS, et al. Persistent pure ground-glass opacity lung nodules ≥ 10 mm in diameter at CT scan: histopathologic comparisons and prognostic implications. Chest 2013;144:1291-9.
9. Jin X, Zhao SH, Gao J, et al. CT characteristics and pathological implications of early stage (T1N0M0) lung adenocarcinoma with pure ground-glass opacity. Eur Radiol 2015;25:2532-40.
10. Li Q, Fan L, Cao ET, et al. Quantitative CT analysis of pulmonary pure ground-glass nodule predicts histological invasiveness. Eur J Radiol 2017;89:67-71.
11. Aoki M, Takai Y, Narita Y, et al. Correlation between tumor size and blood volume in lung tumors: a prospective study on dual-energy gemstone spectral CT imaging. J Radiat Res 2014;55:917-23.
12. Ding H, Shi J, Zhou X, et al. Value of CT Characteristics in Predicting Invasiveness of Adenocarcinoma Presented as Pulmonary Ground-Glass Nodules. Thorac Cardiovasc Surg 2017;65:136-41.
13. Si MJ, Tao XF, Du GY, et al. Thin-section computed tomography-histopathologic comparisons of pulmonary focal interstitial fibrosis, atypical adenomatous hyperplasia, adenocarcinoma in situ, and minimally invasive adenocarcinoma with pure ground-glass opacity. Eur J Radiol 2016;85:1708-15.
14. Wu F, Tian S, Jin X, et al. CT and histopathologic characteristics of lung adenocarcinoma with pure ground-glass nodules 10 mm or less in diameter. Eur Radiol 2017;27:4037-43.
15. Zhang Y, Qiang J, Ye J, et al. High resolution CT in differentiating minimally invasive component in early lung adenocarcinoma. Lung Cancer 2014;84:236-41.
16. Yue X, Liu S, Liu S, et al. HRCT morphological characteristics distinguishing minimally invasive pulmonary adenocarcinoma from invasive pulmonary adenocarcinoma appearing as subsolid nodules with a diameter of </=3 cm. Clin Radiol 2018;73:411.e7-411.e15.
17. Han L, Zhang P, Wang Y, et al. CT quantitative parameters to predict the invasiveness of lung pure ground-glass nodules (pGGNs). Clin Radiol 2018;73:504.e1-504.e7.
18. Song YS, Park CM, Park SJ, et al. Volume and mass doubling times of persistent pulmonary subsolid nodules detected in patients without known malignancy. Radiology 2014;273:276-84.
19. Borghesi A, Farina D, Michelini S, et al. Pulmonary adenocarcinomas presenting as ground-glass opacities on multidetector CT: three-dimensional computer-assisted analysis of growth pattern and doubling time. Diagn Interv Radiol 2016;22:525-33.
20. Kim H, Goo JM, Park CM. Evaluation of T categories for pure ground-glass nodules with semi-automatic volumetry: is mass a better predictor of invasive part size than other volumetric parameters? Eur Radiol 2018;28:4288-95.
21. Zhang Y, Cheng J, Hua X, et al. Can Spectral CT Imaging Improve the Differentiation between Malignant and Benign Solitary Pulmonary Nodules? PLoS One 2016;11:e0147537.

22. Chae EJ, Song JW, Seo JB, et al. Clinical utility of dual-energy CT in the evaluation of solitary pulmonary nodules: initial experience. Radiology 2008;249:671-81.
23. Fischer MA, Gnannt R, Raptis D, et al. Quantification of liver fat in the presence of iron and iodine: an ex-vivo dual-energy CT study. Invest Radiol 2011;46:351-8.
24. Son JY, Lee HY, Kim JH, et al. Quantitative CT analysis of pulmonary ground-glass opacity nodules for distinguishing invasive adenocarcinoma from non-invasive or minimally invasive adenocarcinoma: the added value of using iodine mapping. Eur Radiol 2016;26:43-54.
25. Liu G, Li M, Li G, et al. Assessing the Blood Supply Status of the Focal Ground-Glass Opacity in Lungs Using Spectral Computed Tomography. Korean J Radiol 2018;19:130-8.
26. Zhang Y, Tang J, Xu J, et al. Analysis of pulmonary pure ground-glass nodule in enhanced dual energy CT imaging for predicting invasive adenocarcinoma: comparing with conventional thin-section CT imaging. J Thorac Dis 2017;9:4967-78.
27. Yang Y, Li K, Sun D, et al. Invasive Pulmonary Adenocarcinomas Versus Preinvasive Lesions Appearing as Pure Ground-Glass Nodules: Differentiation Using Enhanced Dual-Source Dual-Energy CT. AJR Am J Roentgenol 2019;213:W114-22.
28. Lee SM, Park CM, Goo JM, et al. Invasive Pulmonary Adenocarcinomas versus Preinvasive Lesions Appearing as Ground-Glass Nodules: Differentiation by Using CT Features. Radiology 2013;268:265-73.
29. Lee HY, Choi Y-L, Lee KS, et al. Pure ground-glass opacity neoplastic lung nodules: histopathology, imaging, and management. AJR Am J Roentgenol 2014;202:W224-33.
30. Park CM, Goo JM, Lee HJ, et al. Nodular ground-glass opacity at thin-section CT: histologic correlation and evaluation of change at follow-up. Radiographics 2007;27:391-408.
31. McCollough CH, Leng S, Yu L, et al. Dual- and Multi-Energy CT: Principles, Technical Approaches, and Clinical Applications. Radiology 2015;276:637-53.
32. Thieme SF, Johnson TR, Lee C, et al. Dual-energy CT for the assessment of contrast material distribution in the pulmonary parenchyma. AJR Am J Roentgenol 2009;193:144-9.
33. Park J, Choi YH, Cheon JE, et al. Advanced virtual monochromatic reconstruction of dual-energy unenhanced brain computed tomography in children: comparison of image quality against standard mono-energetic images and conventional polychromatic computed tomography. Pediatr Radiol 2017;47:1648-58.
34. Wang Y, Qian B, Li B, et al. Metal artifacts reduction using monochromatic images from spectral CT: evaluation of pedicle screws in patients with scoliosis. Eur J Radiol 2013;82:e360-6.
35. Horat L, Hamie MQ, Huber FA, et al. Optimization of Monoenergetic Extrapolations in Dual-Energy CT for Metal Artifact Reduction in Different Body Regions and Orthopedic Implants. Acad Radiol 2019;26:e67-e74.

Cite this article as: Yu Y, Cheng JJ, Li JY, Zhang Y, Lin LY, Zhang F, Xu JR, Zhao XJ, Wu HW. Determining the invasiveness of pure ground-glass nodules using dual-energy spectral computed tomography. Transl Lung Cancer Res 2020;9(3):484-495. doi: 10.21037/tlcr.2020.03.33

